

Supplementary data

STING Activation Reprograms Tumor Vasculatures and Synergizes with VEGFR2 Blockade

Hannah Yang, Won Suk Lee, So Jung Kong, Chang Gon Kim, Joo Hoon Kim,
Sei Kyung Chang, Sewha Kim, Gwangil Kim, Hong Jae Chon, and Chan Kim

Supplementary Table 1. Clinicopathologic characteristics of patient cohorts

Breast cancer (n=173)			Colorectal cancer (n=160)		
		n (%)			n (%)
Sex	Male	0 (0)	Sex	Male	85 (53.1)
	Female	173 (100.0)		Female	75 (46.9)
Age (mean ± STD)		49.6 ± 11.8	Age (mean ± STD)		61.5 ± 12.5
Stage	I	58 (33.5)	Stage	I	13 (8.1)
	II	80 (46.2)		II	65 (40.6)
	III	34 (19.7)		III	81 (50.6)
	IV	1 (0.6)		IV	1 (0.6)
Grade	G1	26 (15.0)	Differentiation	WD and MD	136 (85.0)
	G2	64 (37.0)		PD	9 (5.6)
	G3	83 (48.0)		Others	15 (9.4)
LVI	No	82 (47.4)	LVI	No	118 (73.8)
	Yes	91 (52.6)		Yes	42 (26.3)
ER+		106 (61.3)	MSI	MSS	92 (78.6)
PR+		87 (50.3)		MSI-low	10 (8.5)
HER2+		39 (22.5)		MSI-high	15 (12.8)
Recurrence	No	138 (79.8)	Recurrence	No	121 (76.1)
	Yes	35 (20.2)		Yes	38 (23.9)
Death	No	145 (83.8)	Death	No	100 (62.5)
	Yes	28 (16.2)		Yes	60 (37.5)
Follow-up duration (median, range)		86, 1-124	Follow-up duration (median, range)		85, 0-192

STD, standard deviation; LVI, lymphovascular invasion; WD, well-differentiated; MD, moderately-differentiated; PD, poorly differentiated; ER, estrogen receptor; PR, progesterone receptor; HER2, human epidermal growth factor receptor 2; MSI, microsatellite instability; MSS, microsatellite stable.

Supplementary Table 2. Prevalence of lymphovascular invasion (LVI) in breast and colorectal cancer patients. P values by chi-square test.

Breast cancer		Endo STING		Colorectal cancer		Endo STING	
		Low	High			Low	High
LVI	No	66.2%	80.7%	LVI	No	38.6%	59.3%
	Yes	33.8%	19.3%		Yes	61.4%	40.7%
<i>P</i> = 0.037				<i>P</i> = 0.007			

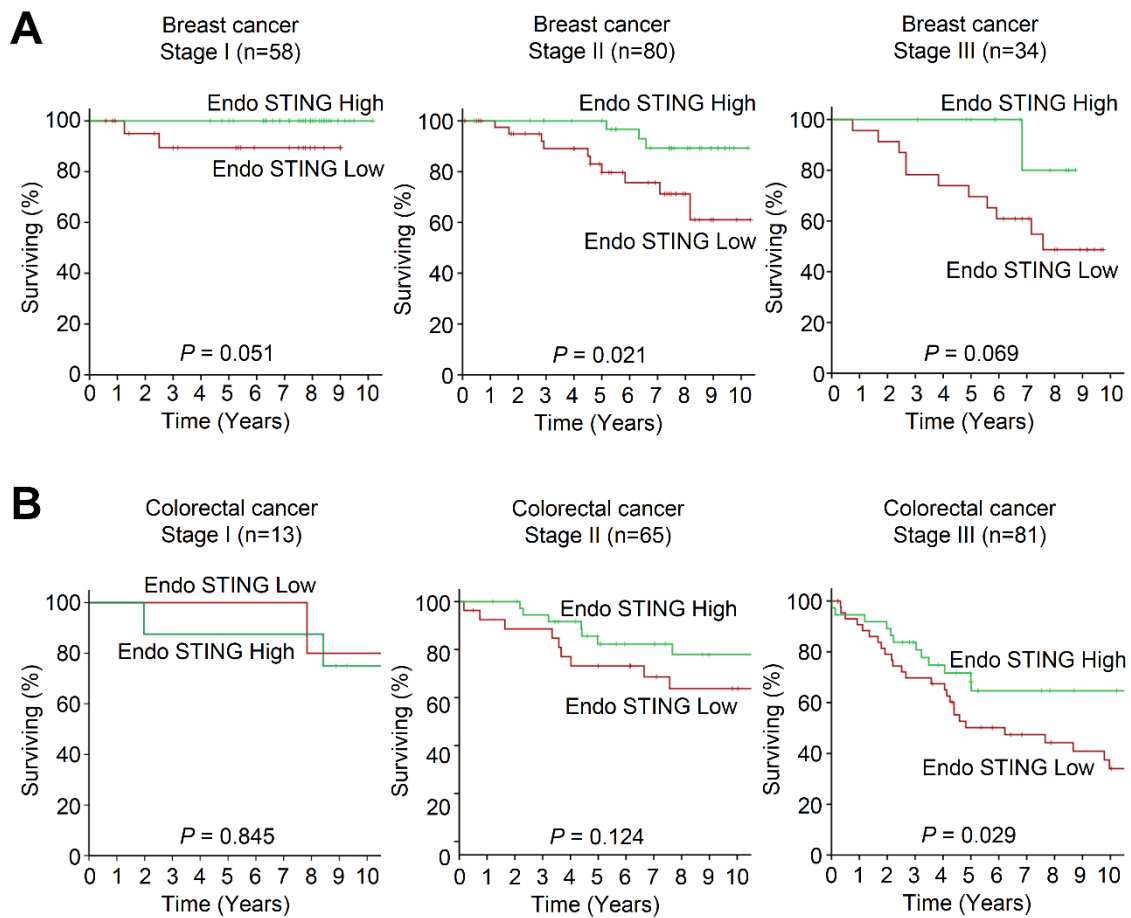
Supplementary Table 3. Multivariate Cox regression analyses for overall survival

Breast cancer

Clinicopathologic variables	HR (95% CI)	P-value
Age (≥ 65 or < 65)	3.927 (1.539-10.019)	0.004
Stage (III, IV or I, II)	2.427 (0.981-6.007)	0.055
Grade (3 vs. 1,2)	2.223 (0.868-5.692)	0.096
Endothelial STING (High vs. Low)	0.175 (0.058-0.526)	0.002
LVI (Present vs. Absent)	0.881 (0.315-2.458)	0.808
ER/PR (Positive vs. Negative)	0.827 (0.358-1.909)	0.657
HER2 (Positive vs. Negative)	1.353 (0.608-3.010)	0.459

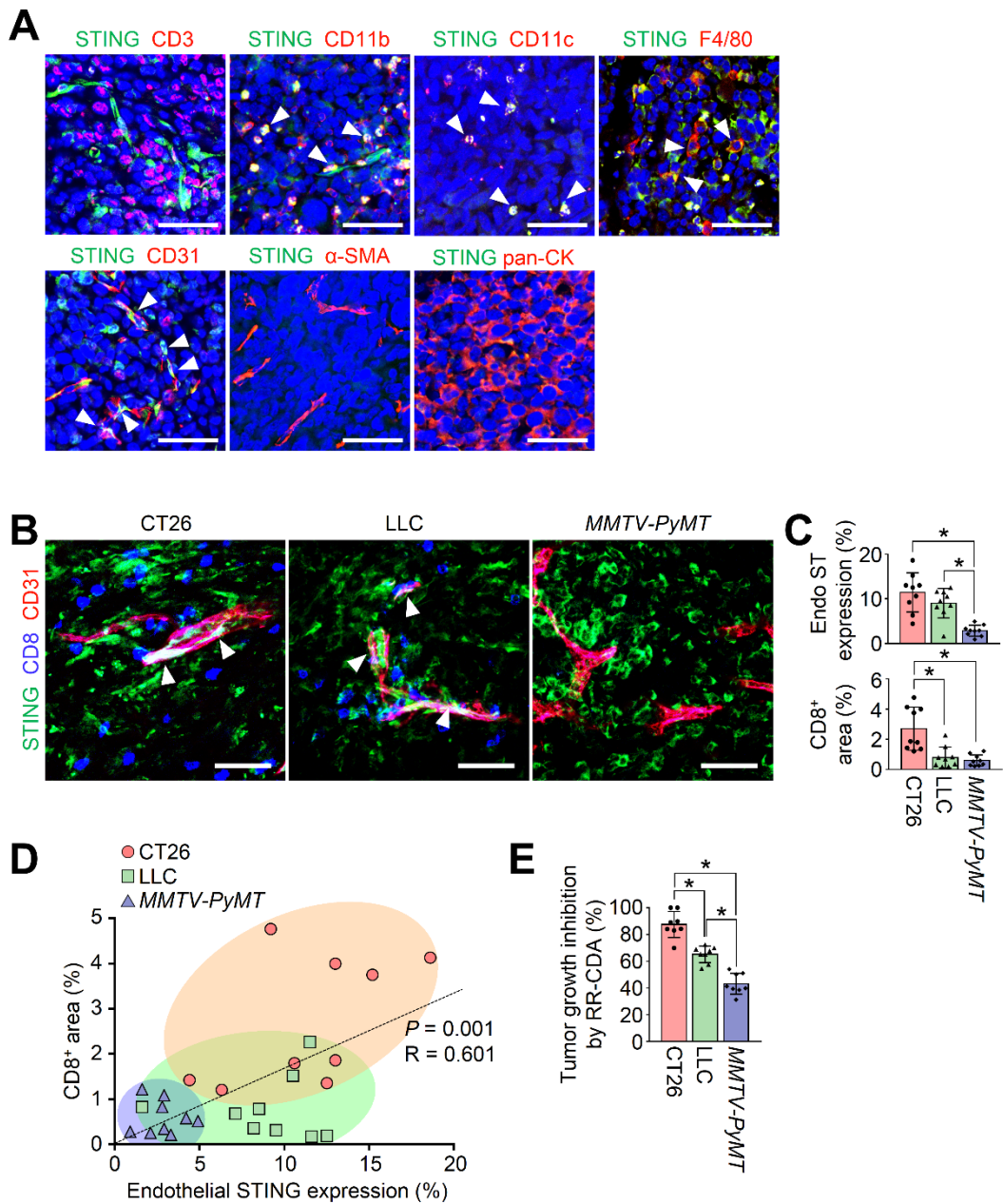
Colorectal cancer

Clinicopathologic variables	HR (95% CI)	P-value
Age (≥ 65 or < 65)	1.399 (0.731-2.678)	0.311
Stage (III, IV or I, II)	1.810 (0.892-3.671)	0.100
Differentiation (APD vs. WMD)	1.197 (0.494-2.897)	0.691
Endothelial STING (High vs. Low)	0.509 (0.262-0.991)	0.047
LVI (Present vs. Absent)	1.820 (0.901-3.676)	0.095
MSI (MSI-H vs. MSS/MSI-L)	0.747 (0.224-2.488)	0.635



Supplementary Figure 1. Endothelial STING expression correlates with favorable prognosis for all stages in human cancers.

(A–B) Kaplan-Meier survival curves of breast cancer patients (A) and colorectal cancer patients (B) according to endothelial STING expression (Endo STING). *P* values by log-rank test.



Supplementary Figure 2. Endothelial STING expression correlates with intratumoral CD8⁺ T-cell infiltration and therapeutic efficacies of STING agonist in various mouse tumor models.

CT26 colon or LLC lung tumor cells were implanted subcutaneously into mice and their tumor growth was monitored. In a spontaneous *MMTV-PyMT* breast cancer, tumor growth was measured starting from 9 weeks after birth. All tumors were analyzed for STING and CD8 expression.

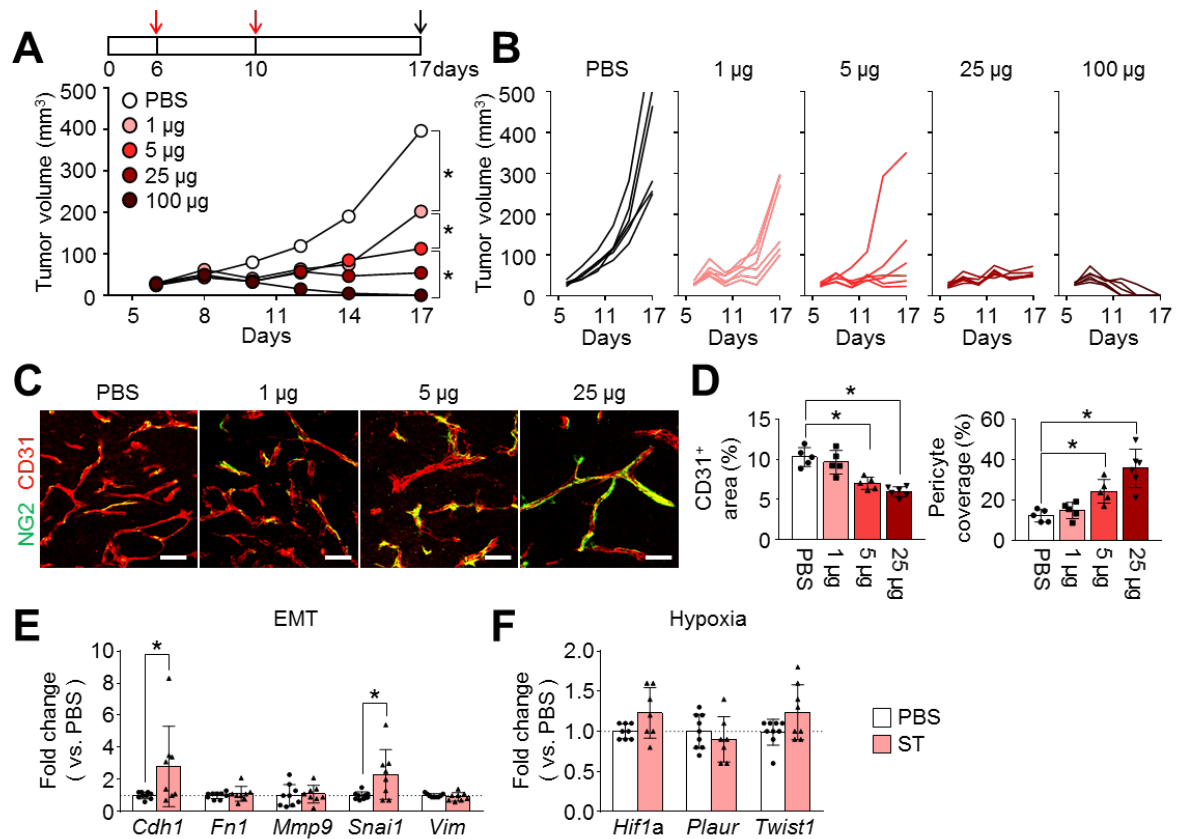
(A) STING expression was assessed in various cell types including CD3⁺ lymphocytes, CD11b⁺ myeloid cells, CD11c⁺ dendritic cells, F4/80⁺ macrophages, CD31⁺ endothelial cells, SMA⁺ pericytes, and pan-CK⁺ tumor cells in LLC tumor. White arrowheads indicate STING-expressing cells.

(B–C) Representative images (B) and comparisons (C) of STING-expressing tumor vessels (Endo STING) (arrowheads) and intratumoral CD8⁺ T cells (blue).

(D) Correlation between endothelial STING expression and intratumoral CD8⁺ T cells in mouse tumor models.

(E) Comparisons of tumor growth inhibitions in mice treated with STING agonist. Mice were treated with intratumoral injections of PBS or a STING agonist (RR-CDA, 25 µg) twice in a three-day interval when the tumors reached >4–5mm in diameter. The inhibition of tumor growth by STING agonist compared with PBS-treated tumors was calculated four days after the last treatment.

Each group, n = 8 to 9. Values are mean ± SD. **P* < 0.05. ANOVA with Tukey post-hoc test (C and E). Pearson correlation test (D). Scale bars, 50 µm.



Supplementary Figure 3. STING agonist regulates tumor growth and tumor vasculature in a dose-dependent manner.

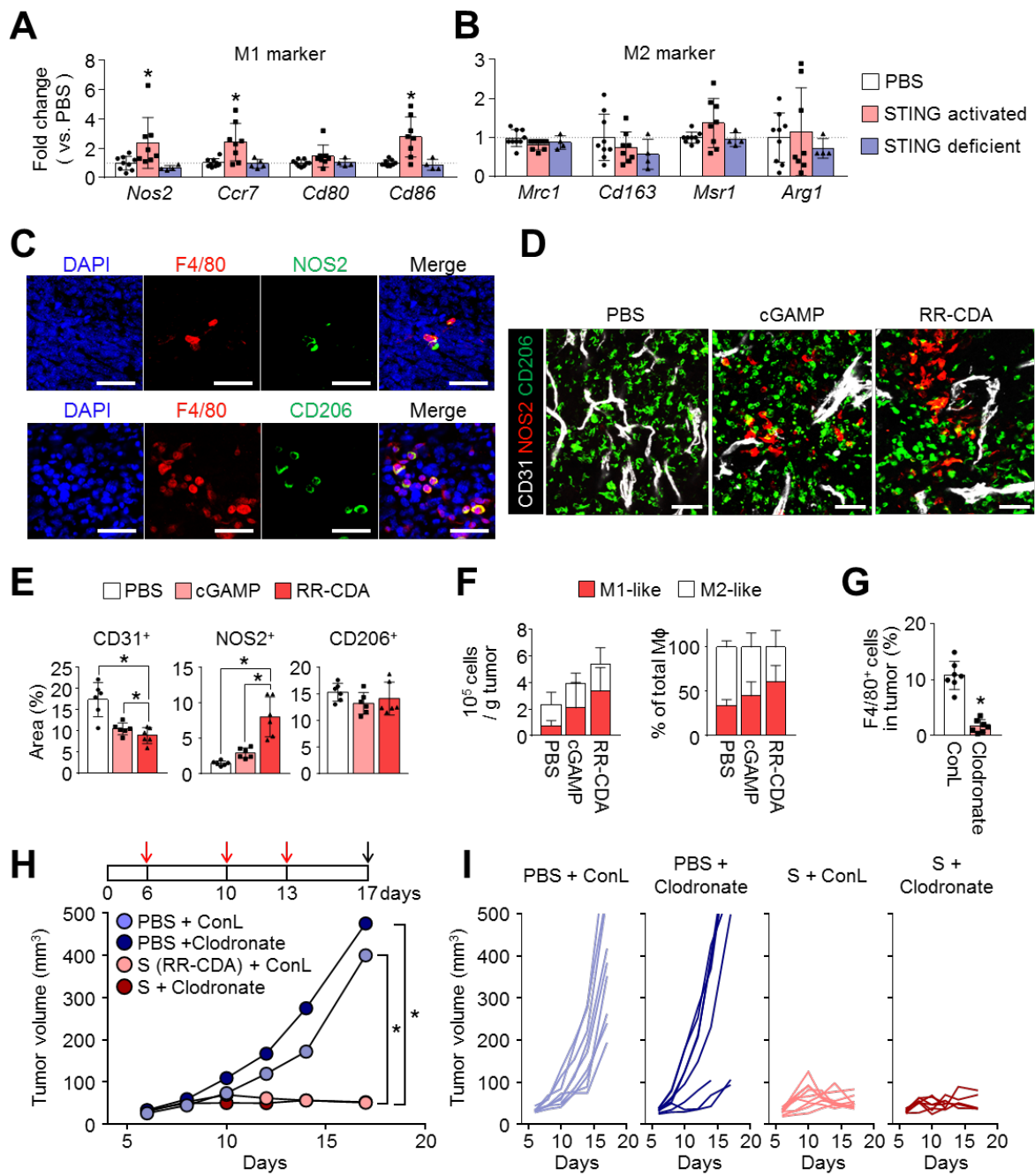
(A–D) Mice were subcutaneously implanted with LLC tumor cells and treated with different doses of RR-CDA (0, 1, 5, 25, and 100 µg). Each group, n = 6.

(A–B) Comparison of LLC tumor growth. Mean (A) and individual (B) tumor growth curves over time. Red arrows indicate treatment and black arrow indicates the sacrifice of mice.

(C–D) Representative images (C) and comparisons (D) of CD31⁺ blood vessels and NG2⁺ pericyte coverage. Scale bars, 50 µm.

(E–F) Comparison of gene expressions related to EMT (E) and hypoxia (F) in tumors treated with PBS or cGAMP. n = 8 to 9.

Values are mean ± SD. **P* < 0.05. ANOVA with Tukey post-hoc test (A and D). Two-tailed Student *t*-test (E and F).



Supplementary Figure 4. STING agonists promote M1-like macrophage accumulation in tumors.

(A–B) Comparison of gene expressions related to M1- (A) or M2- (B) macrophage polarization in STING-activated or STING-deficient tumors.

(C) Representative images of F4/80⁺NOS2⁺ M1-like macrophages and images of F4/80⁺CD206⁺ M2-like macrophages in LLC tumors.

(D–E) Representative images **(D)** and comparisons **(E)** of CD31⁺ blood vessels, NOS2⁺ M1-like macrophages, and CD206⁺ M2-like macrophages after intratumoral treatment of STING agonist (cGAMP, 10 µg, or RR-CDA, 25 µg). Each group, n = 6. Scale bars, 50 µm.

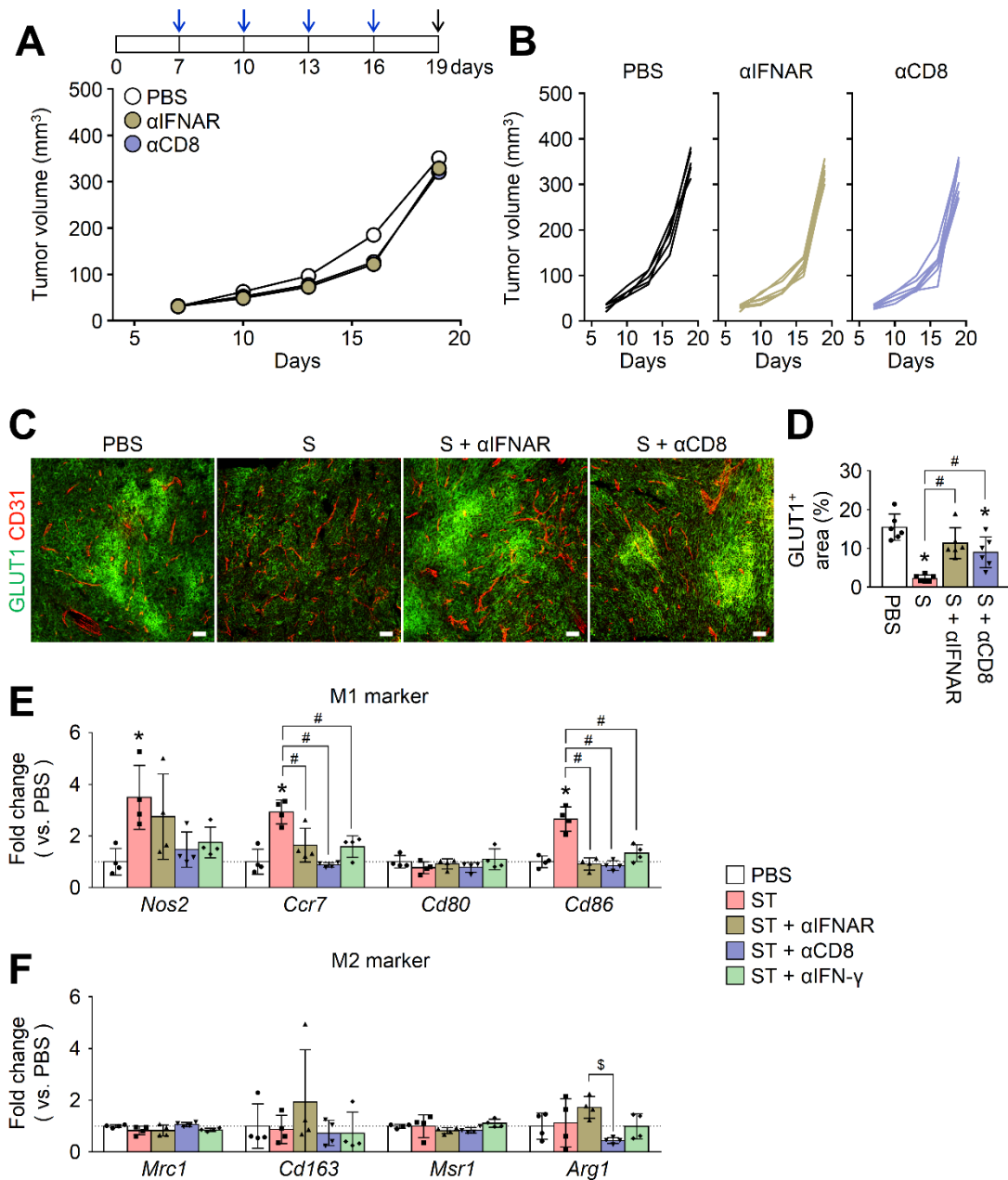
(F) Flow cytometric analyses of M1- and M2-like macrophages in tumors.

(G–I) LLC tumor cells were subcutaneously implanted and treated with intratumoral STING agonist (RR-CDA, 25 µg) or PBS, and intraperitoneal clodronate liposome or control liposome (ConL) (200 µl, three times).

(G) Depletion of intratumoral F4/80⁺ macrophages after clodronate liposome treatment. Each group, n = 7.

(H–I) Mean **(H)** and individual **(I)** tumor growth curves over time. Red arrows indicate injections of STING agonist and/or clodronate liposome and black arrow indicates the sacrifice of mice. Each group, n = 5 to 9.

Values are mean ± SD. **P* < 0.05. Two-tailed Student *t* test (**A**, **B** and **G**). ANOVA with Tukey post-hoc test (**E**).



Supplementary Figure 5. STING agonists alleviate intratumoral hypoxia and regulate genes related to macrophage phenotypes.

LLC tumor cells were implanted subcutaneously into mice and treated with intratumoral injections of PBS or STING agonist (S) and/or depleting antibodies for IFNAR (α IFNAR), CD8 (α CD8), or IFN- γ (α IFN- γ)

(A–B) Comparison of LLC tumor growth in mice treated with intratumoral injections of PBS and/or α IFNAR or α CD8. Mean (A) and individual (B) tumor growth curves over time. Blue

arrows indicate treatment and black arrow indicates the sacrifice of mice.

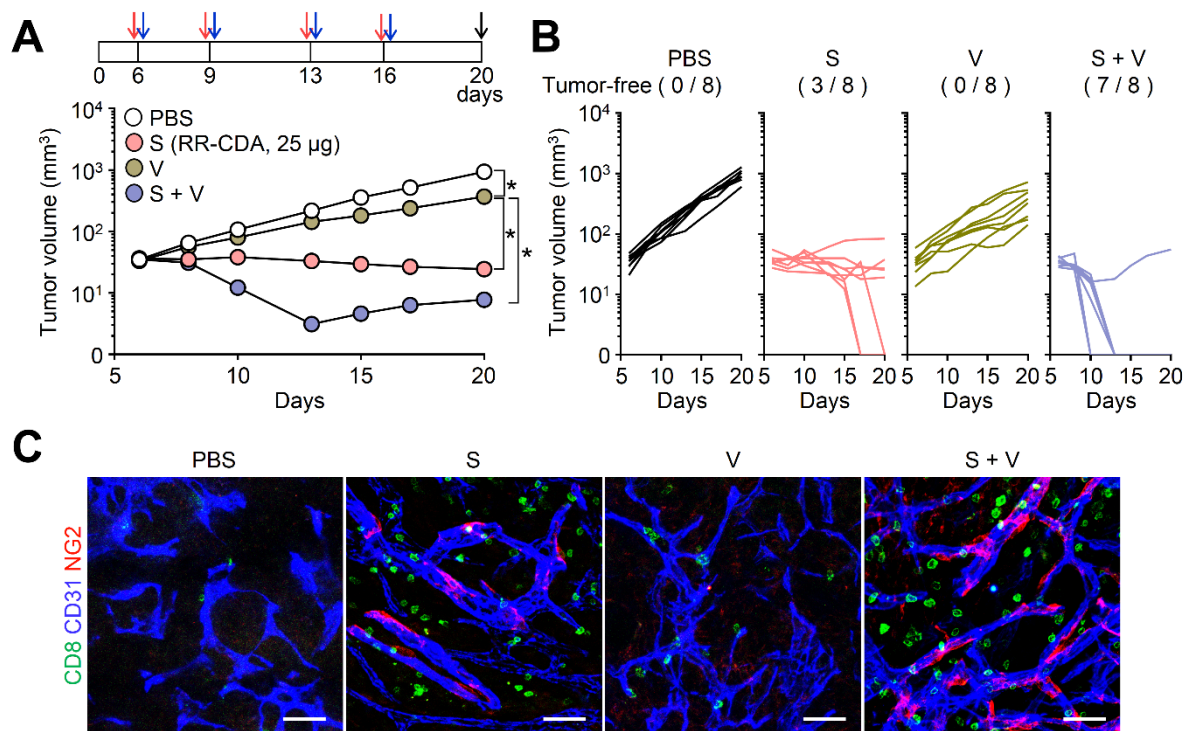
(C–D) Representative images **(C)** and comparisons **(D)** of GLUT1⁺ hypoxic area in tumors.

Each group, n = 6. Scale bars, 50 μm.

(E–F) Comparison of gene expressions related to M1 **(E)** and M2 **(F)** macrophage polarization in tumors. Each group, n = 4.

Values are mean ± SD. **P* < 0.05 versus PBS; #*P* < 0.05 versus S, \$*P* < 0.05 versus S + αIFNAR.

ANOVA with Tukey post-hoc test **(A and D–F)**.



Supplementary Figure 6. STING agonist treatment combined with VEGFR2 blockade induces tumor regression in CT26 tumor model.

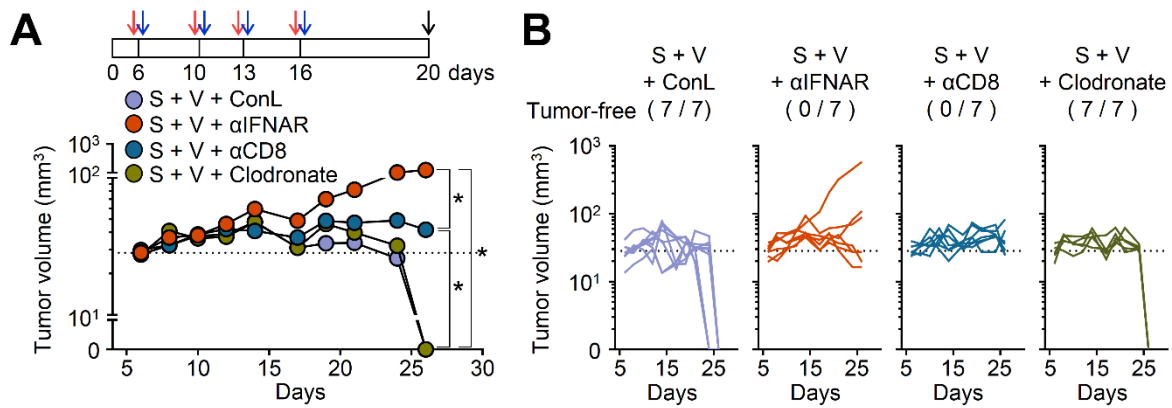
Mice were subcutaneously implanted with CT26 colon cancer cells and treated with STING agonist (S) and/or DC101 (V).

(A–B) Comparison of CT26 tumor growth. Mean (A) and individual (B) tumor growth curves over time. The number of tumor-free mice is indicated for each group. Red arrows indicate injections of S, blue arrows indicate injections of V, and black arrow indicates mice sacrifice.

* $P < 0.05$.

(C) Representative images of CD8⁺ T cells, CD31⁺ blood vessels, and NG2⁺ pericytes in CT26 tumors. Scale bars, 50 µm.

Each group, $n = 8$. ANOVA with Tukey post-hoc test.



Supplementary Figure 7. Efficacy of combination therapy of STING agonist and α VEGFR2 is dependent on type I IFN signaling and CD8⁺ T cells, but not macrophages.

Mice were subcutaneously implanted with LLC tumor cells and treated with a combination treatment of STING agonist and anti-VEGFR2 (S + V) and/or depleting antibodies for IFNAR or CD8⁺ T cells or clodronate liposome.

(A–B) Comparison of tumor growth in mice. Mean (A) and individual (B) tumor growth curves over time. Red arrows indicate injections of RR-CDA (25 μ g) or PBS, and blue arrows indicate injections of depleting antibodies, clodronate liposome, or control liposome (ConL).

Pooled data from two independent experiments with $n = 7$ per group. * $P < 0.05$. ANOVA with Tukey post-hoc test.

Supplementary Methods

Histological analyses. For hematoxylin and eosin (H&E) staining, the tumor and lung tissue samples were fixed overnight in 4% paraformaldehyde (PFA). The tissues were processed using standard procedures. Then the samples were embedded in paraffin, cut into 3- μ m-thick sections, and stained with H&E. For immunofluorescence staining, the tissue samples were fixed in 1% PFA, dehydrated overnight in 20% sucrose solution, and embedded in tissue-freezing medium (Leica). The frozen blocks were sectioned into 50- μ m-thick slices, which were permeabilized with 0.03% PBST (Triton X-100 in PBS), and blocked with 5% donkey or goat serum in 0.01% PBST for 30 min at room temperature (RT). Next, the samples were incubated at RT for 3 h with the following primary antibodies: anti-CD31 (hamster, clone 2H8, Millipore; rabbit, Abcam), anti-CD8 (rat, clone 53-6.7, BD Pharmingen), anti-NG2 (rabbit polyclonal, Millipore), anti-collagen type IV (rabbit polyclonal, Cosmo Bio), anti-GLUT1 (rabbit polyclonal, Millipore), anti-NOS2 (rabbit polyclonal, Abcam), anti-CD206 (rat, clone MR5D3, Invitrogen), anti-PD-L1 (rabbit, clone 28-8, Abcam), anti-Pan-Cytokeratin (Mouse, clone AE1/AE3, DAKO), anti-STING (rabbit, polyclonal, NBP2-24683, Novus biological), anti-F4/80 (rabbit, polyclonal, ab100790, Abcam), or anti-CD11b (rat, clone M1/70, BD Pharmingen). The sections were washed several times, and then incubated for 2 h at RT with the following secondary antibodies: FITC- or Cy3-conjugated anti-rabbit IgG (Jackson ImmunoResearch), FITC- or Cy3-conjugated anti-rat IgG (Jackson ImmunoResearch), Cy3- or Cy5-conjugated anti-hamster IgG (Jackson ImmunoResearch), or FITC-conjugated anti-mouse IgG (Jackson ImmunoResearch). The cell nuclei were counterstained with 4',6-diamidino-2-phenylindole (DAPI, Invitrogen). Finally, the samples were mounted with fluorescent mounting medium (DAKO), and images were acquired using a Zeiss LSM 880 confocal microscope (Carl Zeiss). To detect the hypoxic areas in the tumors, the mice were intraperitoneally injected with Hypoxyprobe-1TM (60 mg/kg, solid pimonidazole hydrochloride,

Natural Pharmacia International) 60 min before sacrifice. After tissue processing as described above, the tumor sections were stained with FITC-conjugated anti-Hypoxyprobe antibody.

Flow cytometry analysis. For flow cytometry analysis, the harvested tumors were minced and then digested into a single-cell suspension by a 1-hour incubation at 37 °C at digestion buffer comprising 2 mg/mL collagenase D (COLLD-RO, Merck) and 40 µg/mL DNaseI (10104159001, Merck). To remove the cell clumps, the suspension was filtered through a 70-µm cell strainer (352350, Corning) and a 40-µm nylon mesh. To remove the red blood cells, the suspension was incubated for 3 min at RT in ACK lysis buffer (A1049201, Fisher Scientific). Next, the cells were incubated on ice for 30 min in Fixable Viability Dye eFluor™ 450 (65-0863-18, Invitrogen) to exclude the dead cells before antibody staining. Then the cells were washed with FACS buffer (1% fetal bovine serum in PBS), and incubated on ice for 30 min in FACS buffer with the following antibodies: FITC-conjugated anti-mouse CD206 (rat, clone MR5D3, Invitrogen), FITC-conjugated anti-mouse PD-1 (armenian hamster, clone J43, Invitrogen), FITC-conjugated anti-mouse CD8a (rat, clone MR5D3, Invitrogen), PE-conjugated anti-mouse CD8a (rat, clone 53-6.7, BD biosciences), PE-conjugated anti-mouse PD-L1 (rat, clone B7-H1, Invitrogen), PE-conjugated anti-mouse TIM3 (rat, clone 8B.2C12, Invitrogen), PerCP/Cy5.5-conjugated anti-mouse Ly-6C (rat, clone HK1.4, Invitrogen), PerCP/Cy5.5-conjugated anti-mouse CD45 (rat, clone 30-F11, Invitrogen), APC-conjugated anti-mouse MHC class II (rat, clone M5/114.15.2, Invitrogen), APC-conjugated anti-mouse CD3 (rat, clone 17A2, Invitrogen), APC-conjugated anti-mouse CTLA-4 (armenian hamster, clone UC10-4B9, Invitrogen), Alexa Fluor 700-conjugated anti-mouse CD11b (rat, clone M1/70, Invitrogen), APC/eFluor 780-conjugated anti-mouse Ly-6G (rat, clone RB6-8C5, Invitrogen), or eFluor 506-conjugated anti-mouse (rat, clone 30-F11, Invitrogen). We analyzed the following cell subsets: M1-like TAM, gated as viability dye⁻/CD45⁺/CD11b⁺/Ly-6G⁻/Ly-

6C⁻/CD206⁺/MHC II^{high} cells; M2-like TAM, gated as viability dye⁻/CD45⁺/CD11b⁺/Ly-6G⁻/Ly-6C⁻/CD206⁻/MHC II^{low} cells; PD-1⁺ T cell, gated as viability dye⁻/CD45⁺/CD3⁺/CD8⁺/PD-1⁺ cells; Tim3⁺ T cell, gated as viability dye⁻/CD45⁺/CD3⁺/CD8⁺/TIM3⁺ cells; CTLA-4⁺ T cell, gated as viability dye⁻/CD45⁺/CD8⁺/CTLA-4⁺ cells; and PD-L1⁺ cell, gated as viability dye⁻/CD45⁻/PD-L1⁺ cells. The stained cells were analyzed using a CytoFLEX flow cytometer (Beckman Coulter), and the data were analyzed with FlowJo software (Tree Star Inc.).

Morphometric analyses. ImageJ software (<http://rsb.info.nih.gov/ij>) was used for density measurements of the blood vessels, T lymphocytes, pericyte coverage, basement coverage, hypoxia area, and GLUT1⁺ area. Blood vessel density was determined by calculating the CD31⁺ area per random 0.49-mm² field of the tumor sections. The degree of cytotoxic T-lymphocyte infiltration was calculated as the percentage of CD8⁺ area per random 0.49-mm² field. NG2⁺ pericyte or collagen type IV⁺ basement membrane coverage was calculated as the percentage of corresponding fluorescent positive length along the CD31⁺ vessels in a random 0.49-mm² field. Hypoxic area was quantified as the percentage of Hypoxyprobe⁺ or GLUT1⁺ area per random 0.49-mm² field as previously described (1). The degree of infiltration of M1- or M2-like macrophages was determined as the percentage of NOS2⁺ or CD206⁺ area per random 0.49-mm² field, respectively. In the *MMTV-PyMT* mice, lung metastasis was quantified by counting the number of tumor colonies per lung section. All the analyses were performed on at least five fields per mouse.

RNA isolation and NanoString gene expression analysis. For NanoString gene expression analysis, we extracted total RNA from the whole tumor tissues using TRIzol (Invitrogen). The RNA quality was verified using a Fragment Analyzer (Advanced Analytical Technologies, IA,

USA). We used 100 ng RNA for immune profiling with a digital multiplexed NanoString nCounter PanCancer Immune Profiling mouse panel (NanoString Technologies). Each 5- μ l RNA sample was hybridized with 8 μ l nCounter Reporter probe in hybridization buffer, and 2 μ l nCounter Capture probes at 65°C for 16–30 h. Excess probes were removed through a two-step magnetic bead-based purification procedure using the nCounter Prep Station (NanoString Technologies). Specific target molecule abundance was quantified using the nCounter Digital Analyzer to count individual fluorescent barcodes, whereby the corresponding target molecules were assessed. Each assay involved a high-density scan encompassing 280 visual fields. Images of the immobilized fluorescent reporters in the sample cartridge were acquired using a CCD camera, and then data were collected using the nCounter Digital Analyzer. Data analysis was performed using nSolver software (NanoString Technologies). The mRNA profiling data were normalized against housekeeping genes and analyzed using R software (www.r-project.org). The Gene Expression Omnibus accession number for the Nanostring is GSE134129.

Generation of chimeric mice. The chimeric mice were generated by irradiating 10–12-week-old wild-type or STING^{gt/gt} C57BL/6 mice with a dose of 10 Gy. Within 24 h, the irradiated mice were reconstituted with 1×10^7 non-irradiated bone marrow cells from either wild-type or STING^{gt/gt} C57BL/6 mice via tail vein injection and left to rest for ≥ 6 weeks. All the chimeric mice had been given drinking water containing 2 mg/ml neomycin sulfate at least 1 week before irradiation, which was switched to plain water at least 2 weeks before tumor implantation.

Reference

1. Park J-S, et al. Normalization of tumor vessels by Tie2 activation and Ang2 inhibition enhances drug delivery and produces a favorable tumor microenvironment. *Cancer Cell*. 2016;30(6):953-67.